Analysis of Superheated Loop Heat Pipes Exploiting Nanoporous Wick Membranes

I-Tzu Chen and Amit Pharkya
School of Chemical and Biomolecular Engineering, Cornell University, Ithaca, NY 14853

Abraham D. Stroock
School of Chemical and Biomolecular Engineering, Cornell University, Ithaca, NY 14853

Kavli Institute at Cornell for Nanoscale Science, Cornell University, Ithaca, NY 14853

DOI 10.1002/aic.14303
Published online in Wiley Online Library (wileyonlinelibrary.com)

The design and analysis of plant-inspired loop heat pipes (LHPs) that would exploit nanoporous membranes to allow for operation with large capillary pressures and superheated liquid are presented. The operating concepts of this superheated loop heat pipe (SHLHP) resemble the transpiration process in vascular plants: reduction of pressure in leaves drives sap flow up from the roots and overcomes gravity, viscous drag, and reduced chemical potential of water in subsaturated soils. We present a model for steady-state operation and a linear response analysis of both the conventional and superheated designs. Our analysis shows that these SHLHPs could: (1) extend the limitations of conventional LHPs imposed by thermodynamic properties of the working fluid, (2) provide efficient heat transfer over long distances and against large accelerations, and (3) allow for operation in a subsaturated state that would eliminate the thermal resistance and entrainment effect of the liquid film of conventional designs. © 2013 American Institute of Chemical Engineers
AIChE J, 00: 000–000, 2013
Keywords: heat-transfer device, loop heat pipe, metastable liquid, phase equilibrium

Introduction

Advances in technologies for transferring heat play a central role in the progress of many fields. For example, the rate of heat transfer can limit the practical speed of integrated circuits, systems for the storage of portable energy, the operational conditions of vehicles, environmental controls in buildings, and efficiency of industrial processes.[1–9] Furthermore, the volume, mass, and complexity of conventional heat exchangers based on sensible heat transfer can place undesirable constraints on these applications.

Among many different technologies transferring heat, heat pipes (HPs)—closed-circuit systems in which a working fluid transfers its latent heat as it cycles between an evaporator and a condenser—have offered an attractive alternative in an array of applications.[10] The central components required for HPs are wick structures that allow for the existence of a pressure difference, ΔP_c (Pa) between the liquid and vapor phases of the working fluid based on capillarity, as described approximately by the Young–Laplace law

$$\Delta P_c = 2\gamma \cos\theta_c / r_p \quad (1)$$

where γ (Pa m) is the surface tension of the liquid, θ_c is the contact angle, and r_p (m) is the radius of the pore. This capillary pressure can drive the working fluid around its cycle if a difference of temperature exists between the evaporator and the condenser. The applications of conventional HPs have been constrained regarding the length (typically, <1 m) and their orientation with respect to gravity or acceleration. The main origins of these limitations are: (1) the use of wicks with large pores ($r_p > 1$ μm) limits magnitude of ΔP_c (e.g., $\Delta P_c < 1$ bar from Eq. 1 with $\gamma = 0.072$ (Pa m) at 25°C and $\theta_c = 0°$ for water on a perfectly wetting surface) such that dry-out of the wick in the evaporator occurs as the viscous pressure drop grows with length of the pipe and the heat load and as the gravitational pressure drop grows with the length of the pipe and adverse acceleration along its axis. (2) The presence of liquid in the vapor path can obstruct the flow of vapor and increase the conductive thermal resistance at the condenser wall.

Loop heat pipes (LHPs) have been developed to extend the limits of conventional HPs.[11,12] To meet the goal of operating effectively over large distance and under any orientation or against acceleration, the main design rules of LHPs (Figure 1a) are[12]: (1) minimization of the distance that the liquid must move within the wick by placing a thin membrane in the evaporator separating macroscopic conduits for the liquid and vapor; such designs allow for the use of smaller pore diameters in the wick without introducing excessive hydraulic resistance. (2) The introduction of a compensation chamber in the cycle; this chamber accommodates excess working fluid and allows the system to adapt to changing heat loads and temperatures. LHPs have been shown to provide robust operation and improved

Correspondence concerning this article should be addressed to A. D. Stroock at ads10@cornell.edu.

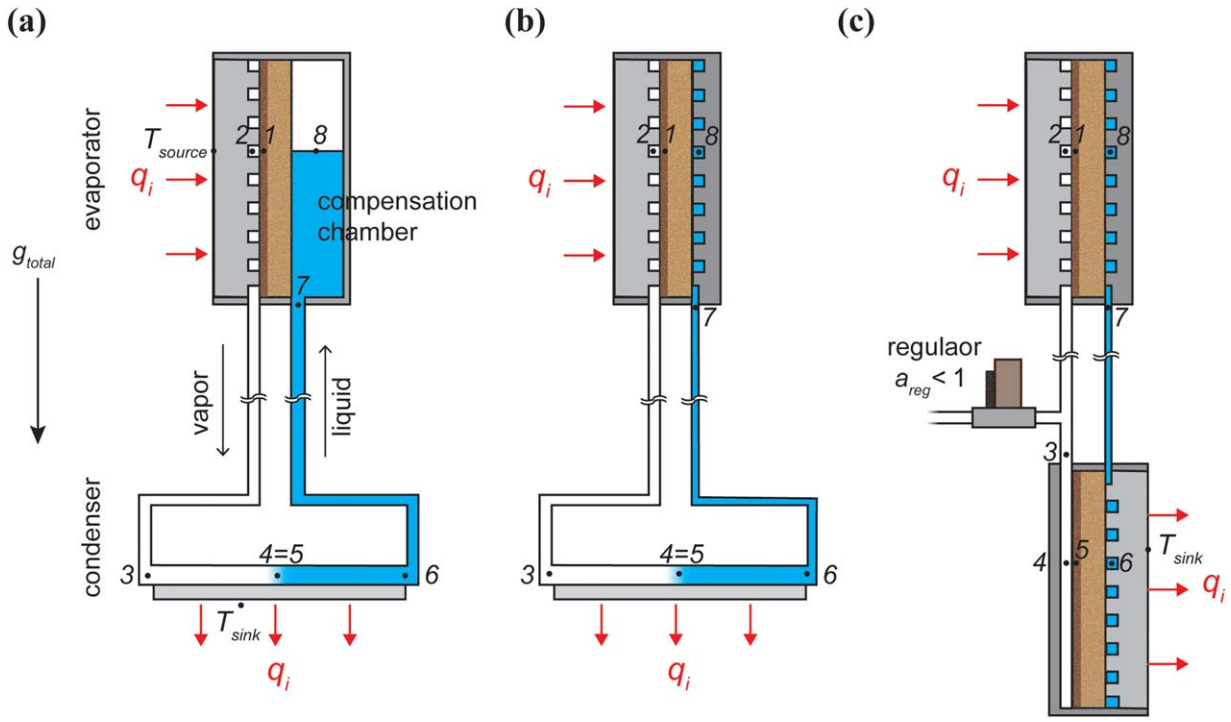

Figure 1. Schematic cross-sectional views of (a) a conventional LHP, (b) a saturated SHLHP, and (c) a subsaturated SHLHP.

An acceleration, g_{total} (m s^{-2}) acts along the pipe axis. Heat enters at the evaporator with a rate q_i (W). The LHP (a) and saturated SHLHP (b) have identical condenser designs. The saturated SHLHP (b) and subsaturated SHLHP (c) have identical evaporator designs with the elimination of the compensation chamber. Nanopoous coatings to allow for subsaturated liquid are shown in all three cases. In the subsaturated SHLHP (c), a regulator connected to the vapor path pins the vapor pressure at an activity of a_{reg}. All the external surfaces except the heat input and output surfaces are assumed to be ideally insulated. The numbers used in this figure corresponds to those used in Figure 2. [Color figure can be viewed in the online issue, which is available at wileyonlinelibrary.com.]

performance relative to conventional HPs, including higher heat load capacities and compatibility with a wider variety of architectures for adaptation to specific applications.[12] However, in conventional LHPs, vapor-liquid coexistence in the compensation chamber forces the thermal cycle to remain close to the saturation and leads to two important constraints[11,13]—the temperature head condition and the subcooling condition—on operation. These constraints can lead to strong dependence of the global thermal resistance of LHPs on the pressure drop along the liquid flow due to viscous drag and adverse acceleration (see the next section for detailed explanations). Additionally, in the condenser of a conventional LHP, the film of condensate can add a significant thermal resistance to the heat transfer, and the unbounded vapor-liquid interfaces can cause undesired oscillations during the startup or in response to heat load steps.[14,15]

In this study, we explore, with a mathematical model, the impact of three modifications of conventional LHPs (Figures 1b, c): (1) reduction of the diameter of pores in the wick membranes such that larger capillary pressures (Eq. 1) can be maintained between the liquid and the vapor. By using nanoporous materials, the maximum capillary pressures could extend to several hundred bars (e.g., $r_p < 10$ nm for water as working fluid). The increased pressure difference developed by fine pores could extend the operational range of LHPs with respect to heat load, length, and adverse acceleration by resisting dry-out from the surfaces of the wicks. (2) Removal of the compensation chamber such that the entire liquid path can become superheated and hence decoupled from the saturation curve. We will illustrate how this superheated loop heat pipe (SHLHP—Figure 1b) would eliminate the temperature head condition and the subcooling condition of conventional designs of LHPs and could substantially decrease the effective thermal conductance at low heat flow and large adverse acceleration. (3) Addition of a nanoporous membrane at the condenser and a regulator of the charge of the pipe such that the entire vapor path and the condenser would remain subsaturated (Figure 1c). The absence of liquid in the vapor path in this subsaturated version of the SHLHP could eliminate the added conductive resistances due to condensate film in the condenser (we characterize this effect) and the instabilities that are observed during changes in heat load (this transient phenomenon lies outside the scope of our steady-state analysis).

There exist a number of foreseeable challenges for the successful realization of both the SHLHP (Figure 1b) and subsaturated SHLHP (Figure 1c). Of particular note are: the potential for increased hydraulic resistance relative to conventional wicks and the increased proneness to dry-out due to boiling along the superheated liquid path. In the next two sections, we discuss specific designs aimed at overcoming these challenges. To motivate the possibility that LHPs could operate reliably with nanoporous wicks and superheat, we note that vascular plants operate with liquid at negative pressures (a superheated state) in their xylem vessels with membranes in their leaves and roots that separate the metastable liquid inside the plant from subsaturated external phases.[16,17] In the process of transpiration (motion of water from the soil to the atmosphere through a plant), a plant serves as a wick:

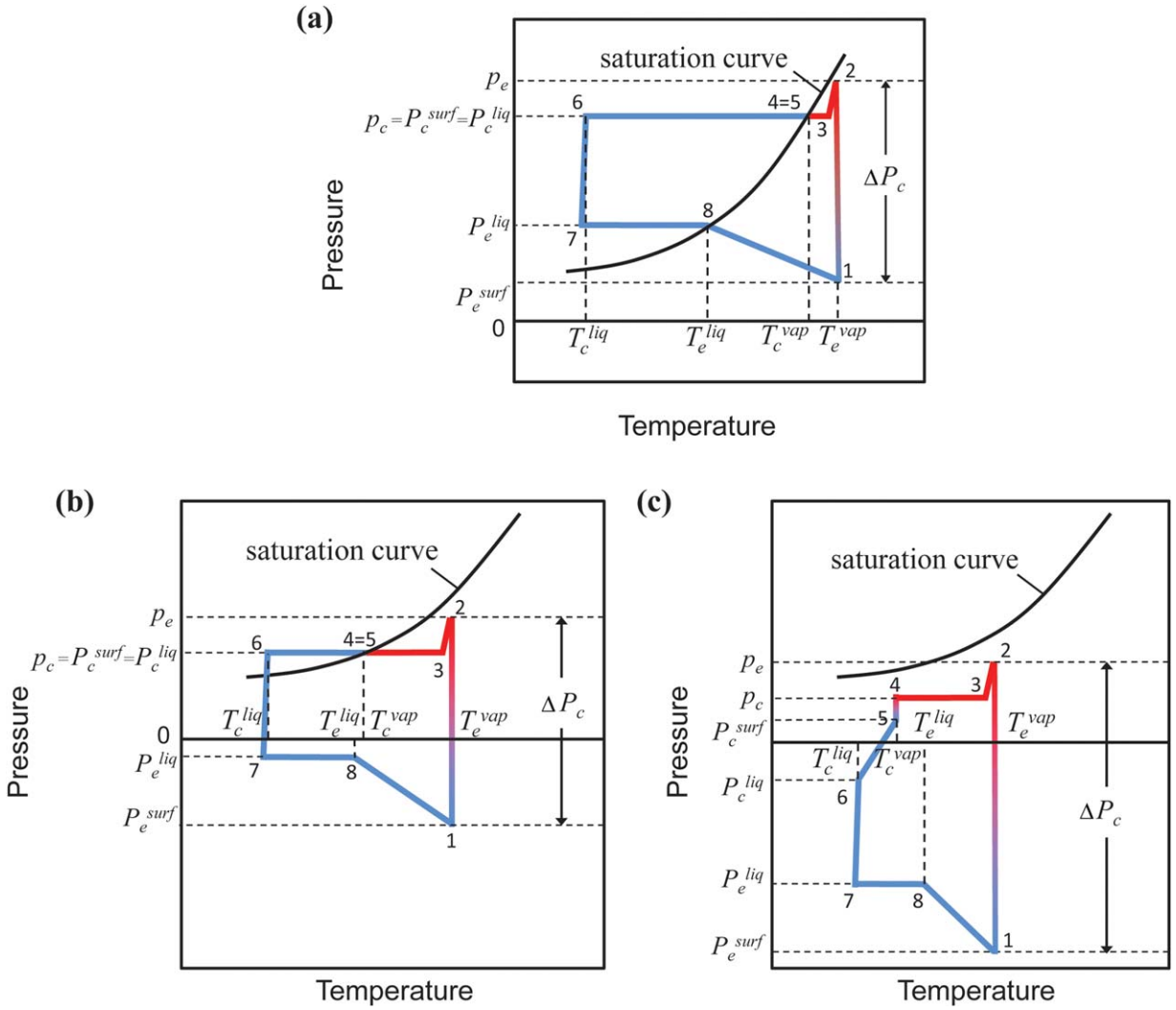

Figure 2. Schematic representations of working cycles on *P-T* diagram for (a) conventional LHPs, (b) saturated SHLHPs, and (c) subsaturated SHLHP.

Points 1–8 correspond to the numbers in Figure 1. The red lines indicate the working fluid is in vapor phase (Path 2–4); the blue lines (Path 5–1) indicate liquid phase. Point 1 represents liquid under the meniscus at the evaporator wick, which is in thermodynamic equilibrium with Point 2, the vapor in the evaporator. Path 2–3 represents the adiabatic motion of the vapor along the vapor path. Point 4 represents vapor in the condenser vapor cavity, in thermodynamic equilibrium with Point 5, the liquid surface in the condenser. Point 6 is liquid before exiting the condenser; Path 6–7 represents motion of the liquid in the liquid path. Point 8 is liquid in the evaporator [in (a), this point is in the compensation chamber]. [Color figure can be viewed in the online issue, which is available at wileyonlinelibrary.com.]

at the leaf (evaporator), reduced pressure in the internal liquid drives flow up from the roots against gravity and the viscous drag in the xylem conduits; in the roots (condenser), reduced pressure transmitted from the leave allows for the extraction of nearly pure liquid from the subsaturated soils or sea water (e.g., in the case of mangroves). Many species operate regularly with pressures down to -50 bars in the liquid water within their xylem.[18] Were a plant enclosed within a fixed volume of vapor, it could act as the liquid path of a subsaturated SHLHP as in Figure 1c. We have demonstrated wicking at large negative pressures in a synthetic system inspired by the operation of plants[19]: using an organic gel as a nanoporous membrane, we showed that water could be transported at steady state from a subsaturated condenser chamber to a further subsaturated evaporator chamber with pressures in the liquid reaching ~ -70 bars. The success of vascular plants in managing superheated liquid and our proof-of-principle demonstration motivate our investigation here of the potential benefits that could be derived from operating LHPs with substantial superheat if boiling and dryout could be avoided. In the Results and Discussion section (*Limits of operation of SHLHP*) and the Conclusions, we discuss the challenges of manipulating superheated liquid.

Design and Operating Principles

Figure 1 shows schematic representations of a conventional LHP (Figure 1a) and two designs of SHLHPs, one with no membrane in the condenser (saturated SHLHP, Figure 1b) and one with an additional membrane in the condenser and a regulator (subsaturated SHLHP, Figure 1c). All three designs separate the liquid and vapor paths such that one can use solid-walled conduits for the vapor and liquid paths instead of having a porous structure throughout. We consider the possibility of nanoporous wick membranes in all three cases. The design of the saturated SHLHP in Figure

1b differs from the conventional design (Figure 1a) only in the elimination of the compensation chamber from the liquid side of the evaporator. This design allows the liquid to become superheated throughout the liquid path, unpinning the liquid in the evaporator (Point 8) from the coexistence curve of the working fluid. This design closely resembles that of conventional HPs (nonloop designs), except for the separation of the liquid and vapor paths by a nonporous wall outside of the evaporator region. Excess liquid volume would collect in the condenser, as in conventional HPs. The subsaturated SHLHP in Figure 1c includes two additional elements: a regulator to maintain a fixed degree of subsaturation in the system and a nanoporous membrane in the condenser. These modifications allow the system to be subsaturated throughout and free from film condensation. Details of these two modifications are described in the next section.

Figure 2 illustrates an idealized form of the working cycles of conventional LHPs (Figure 2a), the saturated SHLHP (Figure 2b), and the subsaturated SHLHP (Figure 2c), with same pressure differences across the vapor path (ΔP_{2-3}) and the liquid path (ΔP_{6-7}) and the same condenser temperature. These cycles will allow us to gain a qualitative understanding of the differences between these designs. The numbered points in the cycles correspond to state of the working fluid at the labeled points in Figure 1. We begin by following the cycle for the conventional case and then point out the important differences in the cycles of the proposed SHLHP designs: In the evaporator, the capillary action holds the meniscus of the liquid in the pores at the wick surface from which evaporation occurs; this liquid is represented as Point 1 and is near thermodynamic equilibrium with Point 2, the vapor in the evaporator. The vapor at Point 2 is slightly subsaturated due to curved menisci (this departure from the saturation curve is often neglected in the literature and Point 2 is placed on the saturation curve). Path 2–3 represents the adiabatic motion of the vapor in the vapor path. As the vapor enters the condenser, the temperature drops until condensation occurs at a macroscopic, vapor-liquid interface on the coexistence line (Point 4 is the vapor; Point 5 is the liquid). Path 5–6 represent subcooling of the liquid before it leaves the condenser. The latent heat released upon condensation is evacuated to a sink. Path 6–7 represents the adiabatic motion of the liquid in the liquid path. As the liquid enters the evaporator at Path 7–8, it is heated by the heat conducted through the wick membrane. Due to the presence of vapor in the compensation chamber, Points 8 is brought to saturation. Path 8–1 corresponds to the liquid motion through the wick membrane to the evaporating meniscus; the liquid confined within the wick membrane becomes superheated.

The working cycle for the conventional design (Figure 2a) illustrates three important conditions for the operation of a conventional LHP[11]: (1) the capillary pressure (ΔP_c) developed by the porous wick must be able to overcome the total pressure drop in the entire loop, including pressure losses in the working fluid along the liquid and vapor paths and through the wick membranes (the pressure losses in the liquid and vapor paths include gravity and accelerations, as in Eqs. A6 and A8)

$$\Delta P_{c,\max} \geq \Delta P^{\mathrm{vap}} + \Delta P^{\mathrm{liq}} + \Delta P^{\mathrm{wick}} \tag{2}$$

(2) The pressure difference between Points 2 and 8, ΔP_{2-8} is responsible for driving the fluid motion through all components except the wick membrane. Given that these two points are saturated (or nearly so for Point 2), their temperature difference is determined by the shape of the coexistence line of the working fluid. This temperature difference must be established across the wick to create the corresponding pressure difference that drives fluid around. This condition has been called the motive temperature head condition[12]

$$\Delta P_{2-8} \cong \left.\frac{dp_s}{dT}\right|_{\overline{T}_e} \Delta T_{2-8} \tag{3}$$

where dp_s/dT is the slope of the coexistence line at the evaporator temperature. (3) The heat leaked through the evaporator wick membrane into the compensation chamber, q_{leak} (W), must be balanced by the sensible heat of returning cold working fluid

$$q_{\mathrm{leak}} = \frac{\Delta T_{2-8}}{R_{\mathrm{wick,e}}} = Q C_p^{\mathrm{liq}} (\Delta T_{8-7}) \tag{4}$$

This balance implies that the temperature difference, ΔT_{8-7} (the subcooling of the liquid before it enters evaporator) grows with increasing ΔT_{2-8} and decreasing the thermal resistance of the evaporator wick, $R_{\mathrm{wick,e}}$. This effect is more pronounced at small heat fluxes for which the mass flow rate Q is small such that a large degree of subcooling is required. To minimize the required subcooling, $R_{\mathrm{wick,e}}$ should be made as large as possible in conventional designs. Combined with Eq. 3, the required subcooling is coupled to the pressure drop across the wick via ΔT_{2-8}; we can call this coupling the subcooling condition.

Figure 2b illustrates the effect of eliminating the compensation chamber from the conventional design in a saturated SHLHP (Figure 1b). Without vapor on the liquid side of the evaporator, Point 8 is no longer constrained to be on the coexistence line. As the demand for pressure drop grows with additional heat load, acceleration or viscous drag, the pressures in the liquid at Points 7, 8, and 1 drop deeper into the superheated region. This use of reduced pressure or even tension (i.e., negative pressure, as presented in Figure 2b) lessens the demand for elevated pressure in the vapor at Point 2, and the temperature head condition (Eq. 3) of the conventional design does not apply. Hence, if evaporator membrane remains wetted and the column of liquid does not cavitate (boil), a small temperature drop throughout the entire device can be achieved and the evaporator temperature of SHLHPs is essentially independent of the hydrostatic pressure load (see the section *Comparison of the response of conventional LHPs and SHLHPs* for justification). A second consequence of allowing Point 8 to drop below the coexistence line is the temperature difference, ΔT_{8-7} remains independent of the load (via Eq. 4 and as the lack of dependence of ΔT_{2-8} on load). This decoupling further allows us to use membrane materials with larger range of thermal conductivities without constraint of the temperature head condition and the subcooling condition. These trends are schematically described in Figure 3, in which the working cycle diagrams are used to illustrate the different response of conventional LHPs and SHLHPs with increasing acceleration load (Figure 3a) and decreasing sink temperature (Figure 3b). Of course, the trade-off for this improved performance of SHLHPs is the extension of the superheated state to the entire liquid path, rather than just the membrane as in the conventional design. In consequence, the total volume of the liquid path should be made as small as possible in a SHLHP to minimize the tendency of the liquid to boiling.

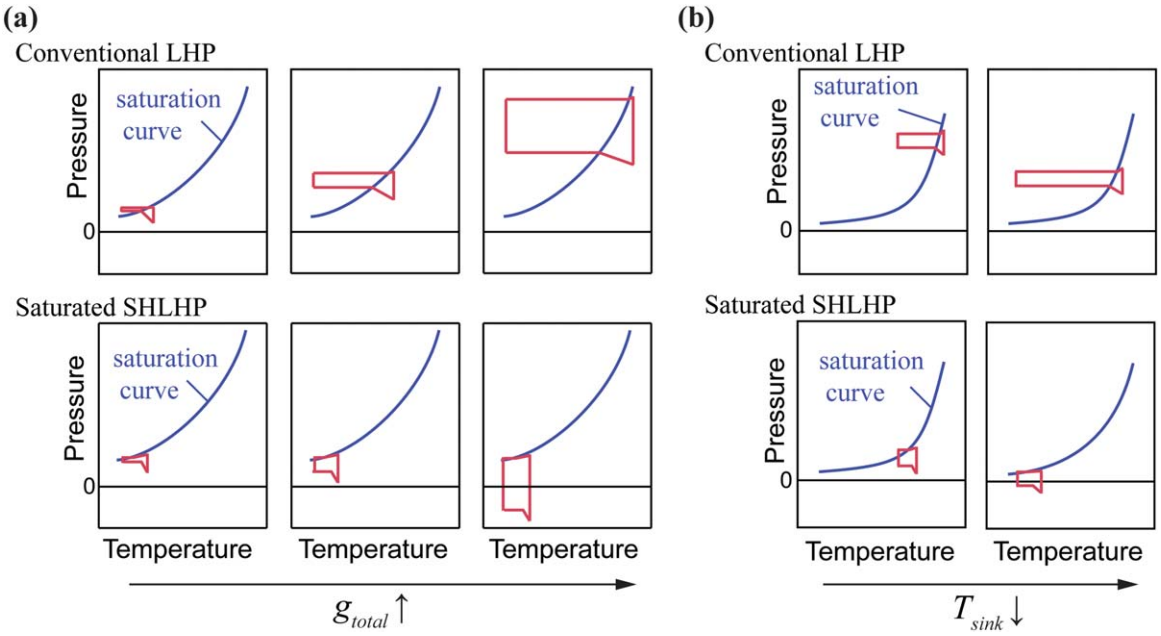

Figure 3. *P-T* diagrams for conventional LHP and SHLHP steady-state operation.

(a) Evolution of the working cycle with increasing adverse acceleration, g_{total}. (b) Evolution of the working cycle with decreasing sink temperature, T_{sink}. For conventional design, corresponding to Eq. 3, as the pressure load goes up, the temperature difference across the evaporator wick goes up (a); as the sink temperature goes down, the slope of coexistence line decreases such that a larger temperature difference is required (b). These demands in the temperature difference across the evaporator wick further affect the subcooling temperature difference, according to Eq. 4. [Color figure can be viewed in the online issue, which is available at wileyonlinelibrary.com.]

Figure 2c illustrates the effects of adding a condenser membrane and a regulator that pins the fluid activity <1 to form a subsaturated SHLHP (Figure 1c, the vapor pressure at Point 4 is controlled by the regulator). In this case, the entire working cycle moves below the saturation line. As our model will illustrate (see *Contributions of loop elements to R_{eff} for SHLHPs*), replacing the saturated condensation process (as in Figures 1a, b) with condensation of subsaturated vapor directly on the nanoporous membrane (Figure 1c) could substantially reduce the temperature drop in the condenser (smaller ΔT_{5-6} in Figure 2c compared to Figure 2b). Under subsaturated conditions, the thermal resistance associated with the condenser is just that of conduction through the wetted membrane. A condenser membrane with low thermal resistivity is, therefore, desirable in a subsaturated design. Eliminating liquid from the vapor path could also mitigate entrainment limitations and complex transients in the two phase regions (our model does not attempt to capture either of these effects).[10,14] Nevertheless, the total pressure drop (ΔP_c) in a subsaturated SHLHP would be larger than those in the conventional or saturated designs, due to the additional membrane in the condenser.

In summary, the important characteristics of the proposed SHLHPs are the large pressure differences between the liquid and vapor phases, the allowance of superheated liquid in the liquid path, and the possibility to work completely below the saturation curve. As we will demonstrate below, these characteristics could improve the performance of LHPs by unpinning the liquid from saturation curve and allowing the system to be subsaturated throughout.

Specifics of Subsaturated SHLHP Design

The global design of a subsaturated SHLHP is similar to that of reversible loop heat pipes[20] in which the vapor and liquid paths are separate and there are wick membranes in both the evaporator and condenser. The structure of the condenser and the evaporator can be designed to be identical to one another such that a subsaturated SHLHP could operate upon reversal of a heat flow, for example, due to changes in environmental conditions. The condenser membrane serves to allow for reduced pressure (below the coexistence pressure) in the liquid in the condenser. This reduced pressure will ensure that the vapor in the condenser remains subsaturated and free of liquid. The regulator replaces the compensation chamber in this design. Whereas the compensation chamber pins the working fluid to the coexistence line in the evaporator, the proposed regulator would pin the chemical potential of the vapor at a subsaturated value at a position along the vapor path.

Nanoporous membrane

Basic requirements of membrane materials for SHLHPs (evaporator membrane in saturated design and both evaporator and condenser membranes in subsaturated design) are similar to those of conventional HPs, including large permeability, high elastic modulus (to sustain pressure differences between the liquid and vapor compartments), and compatibility with the desired range of working temperatures. Moreover, to generate the large ΔP_c (Eq. 1) required for SHLHPs, the pore size should be of submicrometer scale (e.g., for 20 bars of pressure difference with water as room temperature, a pore diameter less than $\sim$100 nm is required at the liquid-vapor interface based on Eq. 1). As mentioned in the Design and Operating Principles section, the thermal conductivity of the evaporator membrane material in SHLHPs does not affect the performance of the system. On the other hand, the condenser membrane material in a subsaturated SHLHP

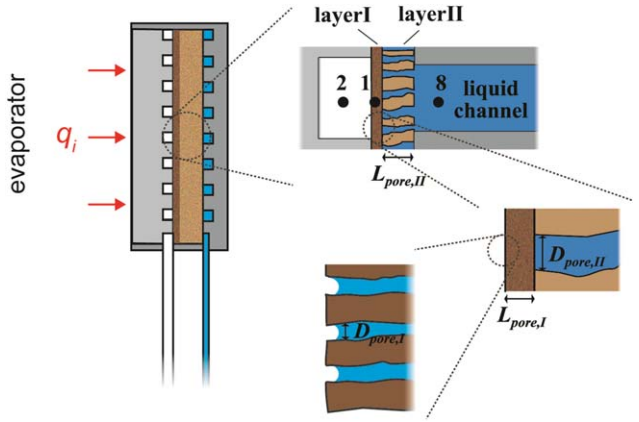

Figure 4. Schematic diagrams of the nanoporous membranes required in the evaporator of the saturated SHLHP and in both the evaporator and condenser of the subsaturated SHLHP.

Expanded cross-sectional views show the wick membranes with a thin coating of a nanoporous material (layer I) connected to a microporous membrane (layer II). The nanoporous layer I has a pore diameter of $D_{pore,I}$ (m), thickness of $L_{pore,I}$ (m), and is supported by layer II with a span $D_{pore,II}$; layer II, thickness of $L_{pore,II}$ (m), supported by the connecting liquid channel. The pores in layer I hold the menisci that define the vapor-liquid interface. [Color figure can be viewed in the online issue, which is available at wileyonlinelibrary.com.]

should be highly conductive to minimize the thermal resistance between the condenser and the heat sink.

Figure 4 presents an enlarged view of Figure 1c, highlighting the nanoporous membrane in the evaporator. As indicated, we propose a layer of nanoporous membrane (layer I) be supported by a microporous layer (layer II) that connects to extended microchannels. The nanoporous layer allows for the generation of large ΔP_c between the liquid and vapor phases; the supporting layer with micrometer scale pores presents a high permeability to flow of the liquid and serves as a structural support of the nanoporous layer. In considering the structural stability of the membranes, we note that the large pressure difference across the membrane could cause the membrane to deform and potentially crack. As the thickness of the membrane decreases (to minimize the hydraulic resistance), the possibility of membrane collapse increases. The micropores of the layer II must be of sufficiently small radius to avoid collapse of layer I. Further, the width of microchannels on the liquid and vapor sides of the membrane should also be sufficiently small to avoid deformation of the whole membranes.

Organic gels or inorganic sol-gels are candidates for the nanoporous coating. Such gels present molecular-scale pores that can provide large capillary pressures. A successful example of using this kind of material is found in the work from Wheeler and Stroock.[19] In that work, an organic gel allowed for capillary pressures in excess of 200 bars. Other candidate materials include nanoporous semiconductors (e.g., porous silicon[21–23]), ceramics,[24] and metals.[25,26] Appropriate candidate materials should have the following properties: (1) high thermal conductivity of the condenser membrane, (2) high mechanical modulus ($\geq$10 GPa), (3) tunablity of pore structure to enable, for example, the formation of membranes with gradients of pore diameter, (4) favorability of surface chemistry with respect to wetting by liquids for stabilization of liquid state with respect to heterogeneous cavitation of superheated liquid, and (5) compatibility with microfabrication techniques allowing for control in geometry and structure of the device and integration of elements of sensing and actuation.

Regulator

To avoid the presence of liquid in the vapor path and saturated liquid film in the condenser, one must regulate the quantity of fluid circulating through the system and control the chemical potential of the system. The inclusion of a regulator coupled to the SHLHP along either the vapor path or the liquid path can achieve this regulation: (1) the regulator acts as a reservoir that accommodates changes of the density of the liquid due to changes in temperature (in the absence of such a regulator, the expansion of fluid with rising temperatures during operation would lead to saturation of the vapor path, even if the system had been charged to a subsaturated level at ambient temperature). Additionally, unlike the compensation chamber in conventional LHPs, the regulator for SHLHP would not contain a vapor-liquid interface. (2) The chemical potential of the fluid controlled by the regulator, μ_{reg} (J mole^{-1}), is maintained at a value less than the standard chemical potential, $\mu_0(T)$, thus maintaining a subsaturated state throughout the SHLHP.

In the design shown in Figure 1c, the regulator is in the vapor path. By connecting the vapor path at the condenser with a pressure controller, one could adjust the vacuum level to regulate the vapor pressure, such that

$$a_{reg} = \frac{p_c}{p_s(T_c^{vap})} \sim \text{constant} < 1 \tag{5}$$

For $a_{reg} < 1$, $\mu_{reg} < \mu_0$. A vapor supply inlet is also located in the vapor path to allow the system to adapt to decreases of applied power.

The regulator could also be located in the liquid path at the condenser. For example, the regulation of a SHLHP with water as the working fluid may be achieved as follows: the pure liquid water in the condenser is coupled via an osmotic membrane to a solution of temperature-independent water activity, $a_{reg} \sim \text{constant} < 1$. Here, the water activity is defined as the mole fraction of water in solution

$$a_{reg} = \frac{[\text{water}]}{[\text{water}] + [S(\text{aq})]} \tag{6}$$

where the brackets represent concentration and S represents a solute. The solute should have a nearly temperature-independent solubility constant $K_s = [S(\text{aq})]$ such that $a_{reg} \sim$ constant.[27,28] The osmotic membrane is required to be mechanically robust to large pressure differences and have high liquid permeability and high rejection coefficient. The volume of the regulator must be variable such that it is able to accommodate or to discharge the fluid to regulate the liquid pressure in the liquid path. The response time of this chamber should be fast compared to the transients in temperature to which it is designed to respond.

Model and Analysis for Steady-State Operation

The behavior and characteristics of conventional LHPs under steady-state operation are well known.[13] A number of steady-state models based on one-dimensional heat and momentum balances have been presented.[11,29–31] These

simple models provide useful predictions of steady-state performance of LHPs. There are several more sophisticated models that focus on the evaporator element only, where the steady-state governing equations for heat and fluid flow are solved numerically.[32,33] However, to the best of our knowledge, no steady-state models have included the condition of local thermodynamic equilibrium between the superheated liquid and subsaturated vapor phases. Neglect of this local equilibrium (neglecting departure from the saturation curve) is often reasonable for when the operating conditions remain near saturation throughout.[34] However, to account for the possibility of significant pressure differences between the liquid and vapor phases with nanoporous wicks, we must account explicitly for the local thermodynamic equilibrium between the phases. In this case, significant superheat may arise in the liquid due to resistance to flow, adverse acceleration, or subsaturation; it is the goal of this study to elucidate the impact of this phenomenon on the performance of the HP.

In the analysis of SHLHP, we assume that neither dry-out (entry of vapor) nor cavitation (boiling) occur in the liquid path. We discuss these assumptions in the Results and Discussion section (*Limits of operation of SHLHP*). To model the steady-state operation, we consider heat and momentum balances as in conventional analyses[11,29,35]; unified heat and momentum balance equations for both conventional LHPs and SHLHPs are presented in Appendix A. In the following subsections, we highlight equations for the condition of local equilibrium; we then proceed to linearize these equations to extract expressions for the effective thermal resistance for SHLHPs. The conversion of the nomenclature for temperatures and pressures at different points in the loop can be found in Figure 2.

Local thermodynamic equilibria

Applying the condition of local equilibrium, we set the chemical potentials equal across the interfaces at which phase change occurs: $\mu_w^{surf}=\mu_w^{vap}$. The use of this condition neglects the possibility of interfacial resistance due to, for example, contaminates adsorbed on the interface. With this condition, we can write down explicitly the thermodynamic balance equations at vapor-liquid interfaces. For the evaporator, we set the chemical potentials of the liquid and vapors equal to find

$$\overline{v}_{liq}\left[P_e^{surf}-p_s\left(T_e^{vap}\right)\right]=R_{gas}T_e^{vap}\ln\left[\frac{p_e}{p_s(T_e^{vap})}\right] \tag{7}$$

In deriving Eq. 7, we have assumed that the liquid is inextensible with molar volume, v_{liq} (m^3 $mole^{-1}$) and the vapor acts as an ideal gas.[36]

For conventional LHPs and saturated SHLHPs without wick membrane in the condenser, vapor is in equilibrium with the liquid in the condenser

$$P_c^{surf}=p_c \tag{8}$$

Also, there is negligible curvature of the vapor-liquid interface for conventional LHPs and saturated SHLHP without condenser membranes, such that the pressure of the liquid is simply the saturation pressure at the local temperature, so we have

$$P_c^{surf}=p_s(T_c^{vap}) \tag{9a}$$

For subsaturated SHLHPs with condenser membranes, the thermodynamic balance equations at subsaturated vapor-liquid interfaces, similar to the one for the evaporator wick surface (Eq. 7), is used

$$\overline{v}_{liq}\left[P_c^{surf}-p_s\left(T_c^{vap}\right)\right]=R_{gas}T_c^{vap}\ln\left[\frac{p_c}{p_s(T_c^{vap})}\right] \tag{9b}$$

Finally, in conventional LHPs, the liquid pressure in the liquid cavity in the evaporator is simply the saturation pressure of the temperature in the compensation chamber due to the coexistence of the two phases

$$P_e^{liq}=p_s(T_e^{liq}) \tag{10a}$$

For SHLHPs, the activity of the fluid is controlled by the regulator. If the regulator is located in the vapor side of the condenser, we have

$$\frac{p_c}{p_s(T_c^{vap})}=a_{reg} \tag{10b}$$

if the regulator is located in the liquid side of the condenser

$$\overline{v}_{liq}\left[P_c^{liq}-p_s\left(T_c^{liq}\right)\right]=R_{gas}T_c^{liq}\ln\left[a_{reg}\right] \tag{10c}$$

For SHLHPs without regulator in the condenser to maintain subsaturated condition, $a_{reg}=1$.

Equations A1–A9 and Eqs. 7–10 can be solved numerically to find the operating temperature, T_{source}, as a function of the heat input, q_i, for a given sink temperature, T_{sink}. The numerical solutions presented in the discussion section are solved iteratively by proceeding as follows: we start with initial guesses for T_e^{vap} and Q, and then solve the rest of the unknowns, including p_e. Using this p_e, we solve Eq. 7 for an updated T_e^{vap} and Eq. A2 for an updated Q, and then solve for the rest of the unknowns. We repeat the steps until the relative change in the values of T_e^{vap} less than 10^{-2} and Q less than 10^{-6} from one iteration to the next.

Linear analysis and expression of LHP effective thermal resistance

The global effective thermal resistance, R_{eff} (K W^{-1}), is used to characterize the LHP performance, and can be defined as follows

$$R_{eff}=\frac{T_{source}-T_{sink}}{q_i} \tag{11}$$

In conventional LHPs, experiments and existing models[11,12,29,35] indicate that, in general, R_{eff} depends on the heat flow, q_i; the response is nonlinear. In particular, at low heat flow, the temperature difference (ΔT_{8-7}) required to satisfy the subcooling condition (Eq. 4) dominates and R_{eff} decreases with increasing q_i ("variable conductance mode"); at high heat flow, R_{eff} becomes constant ("fixed conductance mode") as heat transfer in the condenser becomes the limiting resistance.[11] In contrast, in a SHLHP, the subcooling condition is not constrained by pressure load and we expect R_{eff} to be constant for a small to moderate heat flows; the initial response is linear. Based on this expectation, we develop an analytical expression for this constant R_{eff} for SHLHPs. This expression helps to elucidate the effects of the distinct components of the system on the performance of a SHLHP. In the Results and Discussion section (*Validity of SHLHP linear response*), we check the validity of the following linear analysis against complete solutions of Eqs. A1–A9 and Eqs. 7–10.

Linear response is defined as follows

$$T_{\text{source}} - T_{\text{sink}} \propto q_i \tag{12}$$

When this relation holds, R_{eff} for SHLHPs can be written as a function of $(T_e^{\text{vap}} - T_c^{\text{liq}})$ as

$$\begin{aligned} R_{\text{eff}} &= \frac{T_{\text{source}} - T_e^{\text{vap}}}{q_i} + \frac{T_e^{\text{vap}} - T_c^{\text{liq}}}{q_i} + \frac{T_c^{\text{liq}} - T_{\text{sink}}}{q_i} \\ &= R_{\text{wall,e}} + \frac{T_e^{\text{vap}} - T_c^{\text{liq}}}{q_i} + R_{\text{film}} + R_{\text{wall,c}} \end{aligned} \tag{13}$$

By considering the limit of low heat flow and, thus, small temperature difference, we arrive at an expression for R_{eff} in which we can separate out the contributions associated with the evaporator wall, the vapor flow, the liquid flow, the conduction through the wicks in the condenser, and the heat exchange with the heat sink (see Appendix B for details)

$$R_{\text{eff}} = R_{\text{wall,e}} + R_{\text{vap}} + R_{\text{liq}} + R_{\text{wick,c}} + R_{\text{film}} + R_{\text{wall,c}} \tag{14}$$

In Eq. 14, $R_{\text{wall,e}}$ and $R_{\text{wall,c}}$ are the conductive resistances of the evaporator and condenser walls

$$R_{\text{wall,e}} = \frac{L_{\text{wall}}}{k_{\text{wall}} A_{\text{source}}} \text{ and } R_{\text{wall,c}} = \frac{L_{\text{wall}}}{k_{\text{wall}} A_{\text{sink}}} \tag{15}$$

where L_{wall} (m) is the thickness and k_{wall} (W m^{-1} K^{-1}) is the thermal conductivity of the wall in contact with the heat source or the sink. For the saturated SHLHP without a membrane in the condenser, $R_{\text{wick,c}} = 0$, while for subsaturated SHLHP

$$R_{\text{wick,c}} = \sum_{i=1}^{N} \frac{L_{\text{pore},i}}{k_{\text{w},i} A_{\text{w}}}, i = 1, 2, \ldots, N \tag{16}$$

where N is the total number of layers of the wick membrane in the condenser (e.g., in Figure 1c, $N = 2$). R_{film} accounts for the film condensation heat transfer in tubes

$$R_{\text{film}} = 1/h_{\text{film}} A_{\text{sink}} \tag{17}$$

where we take the heat-transfer coefficient h_{film} from the literature[37,38]

$$h_{\text{film}} = 0.76 \left(\frac{2 k_{\text{liq}}{}^3 \rho_{\text{liq}}{}^2 g L}{\eta_{\text{liq}} Q} \right)^{\frac{1}{3}} \tag{18}$$

where k_{liq} (W m^{-1} K^{-1}) is the thermal conductivity of the condensate and η_{liq} (kg m^{-1} s^{-1}) is the viscosity of the condensate. For the subsaturated SHLHP, the condensation occurs directly on the surface of the condenser membrane (with no film), so we take $R_{\text{film}} = 0$.

The important and less obvious predictions that emerge from the linearization are for the contributions of the vapor and liquid paths

$$R_{\text{vap}} = \frac{1}{\lambda \frac{dp_s}{dT}|_{T_0}} \Gamma_{\text{vap}} = \frac{T_0}{\lambda^2 \rho_{\text{vap},0}} \Gamma_{\text{vap}} \tag{19}$$

and

$$R_{\text{liq}} = \frac{\rho_{\text{vap},0}}{\rho_{\text{liq},0}} \frac{1}{\lambda \frac{dp_s}{dT}|_{T_0}} \left(\Gamma_{\text{liq}} + \sum \Gamma_{\text{wick}} \right) = \frac{T_0}{\lambda^2 \rho_{\text{liq},0}} \left(\Gamma_{\text{liq}} + \sum \Gamma_{\text{wick}} \right) \tag{20}$$

where Γ_{vap} and Γ_{liq} are the hydraulic resistances of the vapor and liquid paths, and $\Sigma\Gamma_{\text{wick}}$ is the sum of the hydraulic resistances of the wick membranes through which the liquid flows. We have used the Clausius–Clapeyron relation (neglecting $1/\rho_{\text{liq}}$ relative to $1/\rho_{\text{vap}}$) to arrive at the second equalities in Eqs. 19 and 20. While earlier investigators derived the expression in Eq. 19[39] we are unaware of a previous derivation of Eq. 20. These expressions clarify the importance of the latent heat, the slope of the saturation curve and the fluid viscosity (present in the hydraulic resistance terms) in defining the impact of hydraulic resistances on SHLHP performance. Comparing to the hydraulic resistance in the vapor path, we note that the impact of hydraulic resistance in the liquid path is less by a factor of $(\rho_{\text{vap}}/\rho_{\text{liq}})$ for equivalent hydraulic resistances; this factor is less than 10^{-3} for water up to 100°C. This observation points to the opportunity to use conduits of small caliber for the liquid path as one designs HPs of large dimensions with nanoporous wicks.

Comparison between the R_{eff} of conventional LHPs and SHLHPs

For conventional LHP and saturated SHLHP which have the same condenser design, the terms $R_{\text{wall,e}}$, R_{film} and $R_{\text{wall,c}}$ are the same. The difference of the global thermal resistance of the two designs lies in the expression for R_{vap} and R_{liq}.

For the conventional design, these resistances can be identified by combining the temperature head condition (Eq. 3) and the subcooling condition (Eq. 4)

$$\begin{aligned} R_{\text{vap}} + R_{\text{liq}} &= \frac{T_e^{\text{vap}} - T_c^{\text{liq}}}{q} \\ &= \frac{\Delta T_{2-8}}{q} + \frac{T_e^{\text{liq}} - T_c^{\text{liq}}}{q} \\ &\cong \frac{\Delta P_{2-8}}{Q \lambda \frac{dp_s}{dT}} + \frac{T_e^{\text{liq}} - T_c^{\text{liq}}}{q} \end{aligned} \tag{21}$$

By further replacing $\Delta P_{2-8}/Q$ by the hydraulic resistances and using Clausius–Clapeyron equation, we can get

$$R_{\text{vap}} + R_{\text{liq}} = \frac{T}{\lambda^2 \rho_{\text{vap}}} \Gamma_{\text{vap}} + \frac{T}{\lambda^2 \rho_{\text{vap}}} \left(\Gamma_{\text{liq}} + \Gamma_{\text{wick}} \right) + \frac{T_e^{\text{liq}} - T_c^{\text{liq}}}{q} \tag{22}$$

The third term from the right hand side of Eq. 22 is a nonlinear term associated to the subcooling effect (Eq. 4)

$$\frac{T_e^{\text{liq}} - T_c^{\text{liq}}}{q} = \frac{\Delta T_{8-7}}{q} \cong \frac{\Delta T_{2-8}}{q^2 C_p^{\text{liq}} R_{\text{wick,e}} / \lambda} \tag{23}$$

At small heat flux or small evaporator wick thermal resistance, this term becomes large and can even dominate the global effective thermal resistance.

For comparison to the saturated SHLHP, Eqs. 19 and 20 give us

$$R_{\text{vap}} + R_{\text{liq}} = \frac{T}{\lambda^2 \rho_{\text{vap}}} \Gamma_{\text{vap}} + \frac{T}{\lambda^2 \rho_{\text{liq}}} \left(\Gamma_{\text{liq}} + \Gamma_{\text{wick}} \right) \tag{24}$$

The first term associated with the hydraulic resistance in the vapor path is identical to R_{vap} for the conventional LHP. The second term, R_{liq} associated with the hydraulic resistance in the liquid path, is different from that in conventional LHP (Eq. 22) by a factor of $(\rho_{\text{liq}}/\rho_{\text{vap}})$. This difference comes from the fact that, for a conventional LHP, the vapor

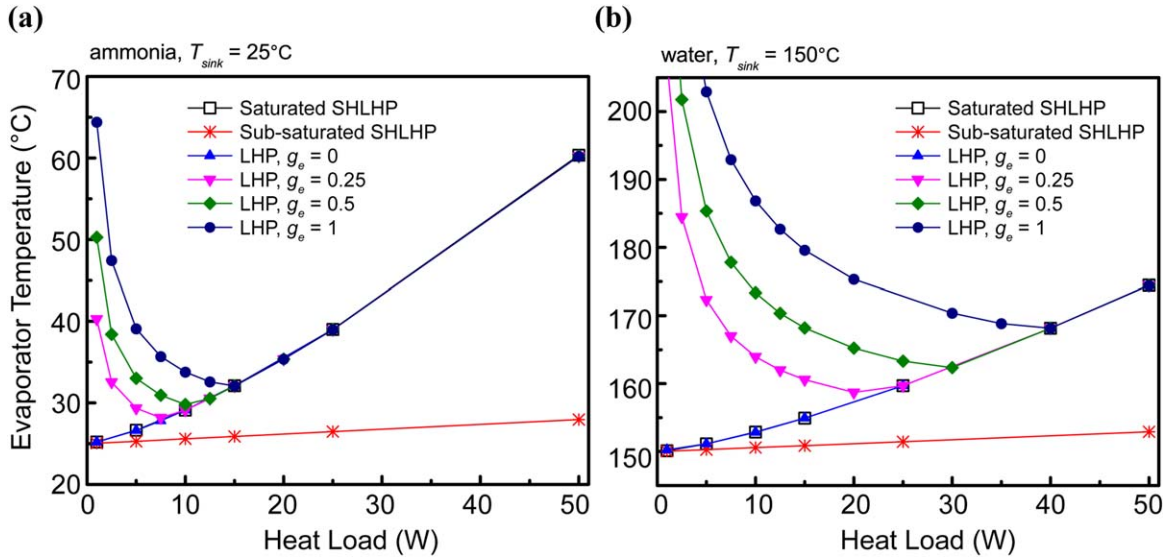

Figure 5. Effect of the adverse acceleration (ranging for 0–1 time gravity) on conventional LHP, saturated SHLHP and subsaturated SHLHP with (a) ammonia and (b) water as working fluid.

Presented data are numerical solutions (Eqs. A1–A9 and Eqs. 7–10). Sink temperature, T_{sink}, is 25°C for (a) and 150°C for (b). Varying g_{total} between 0 and 1 times gravity has no effect on the SHLHPs. The results for saturated LHP overlap with the line for convention LHP at 0 g_e. For the conventional case, $D_{liq} = 1$ mm; for the SHLHPs, $D_{liq} = 350$ μm. Other operational parameters: $L_{pipe} = 10$ m, porosity of the membrane = 0.6, thermal conductivity for the evaporator wick membrane material = 13 W/m K, $D_{vap} = 6$ mm, $L_{pore,1} = 2$ μm, $D_{pore,1} = 20$ nm, $L_{pore,2} = 3$ mm, $D_{pore,2} = 2$ μm, $A_{source} = 1$ cm^{-2}, $L_{wall} = 1$ mm, and $k_{wall} = 400$ W/m K. For saturated condenser, $D_{cond} = 4$ mm, $A_{sink} = 100$ cm^{-2}; for subsaturated SHLHP, a condenser membrane with thermal conductivity = 130 W/m K, $A_w = A_{sink} = 1$ cm^2, $L_{pore,1} = 2$ μm, $D_{pore,1} = 20$ nm, $L_{pore,2} = 300$ μm, and $D_{pore,2} = 2$ μm is added to replace the condenser tube. The vapor pressure in the subsaturated SHLHP is controlled by the regulator and has activity, $a_{reg} = 0.99$. [Color figure can be viewed in the online issue, which is available at wileyonlinelibrary.com.]

pressure in the evaporator must push both the vapor and liquid phases through their respective sections of the loop. In contrast, in the SHLHP, the reduced pressure in liquid in the evaporator drives the liquid flow; the vapor pressure is only responsible for driving the flow of the vapor phase. As we will see in the Results and Discussion section, this distinction leads to significant differences in the responses of the LHP and the SHLHP as the pressure drop along the liquid path increases. The nonlinear term accounting for subcooling (Eq. 23) does not influence the SHLHP because the temperature across the evaporator wick, ΔT_{2-8}, is not directly coupled to the entire pressure drop in the vapor and liquid paths.

Results and Discussion

In Figures 5–9, we present the predictions of the model in the Model and Analysis section for the performance of conventional LHPs and SHLHPs for heat transfer over a distance of 10 m with various operational parameters. The geometries of the systems are as depicted in Figure 1; we take a smaller diameter liquid conduit in the SHLHPs (350 μm diameter) than in the LHPs (1 mm). All parameter values are provided in the captions. The predictions are made by solving Eqs. A1–A9 and Eqs. 7–10 numerically for T_e^{vap} at fixed heat flow and T_{sink} or by evaluating the expressions for effective thermal resistance in Eqs. 14–20.

Comparison of the response of conventional LHPs and SHLHPs

Figure 5 presents the operating curves (steady-state evaporator temperature vs. the heat input) for ammonia (Figure 5a) and water (Figure 5b) with acceleration load, g_{total}, varying from 0 to 1 times gravity ($g_{total} = 0$, 0.25, 0.5, and 1 g_e, where $g_e = 10$ m s^{-2}) for 10-m long pipes. The performance of SHLHPs is essentially independent of acceleration: varying g_{total} has no effect on the performance of either the saturated SHLHP or the subsaturated SHLHP. The operating curves of the saturated SHLHP overlaps with the curve for conventional LHP at $g_{total} = 0$. At high heat flux, the effective thermal resistances of both designs are dominated by the thermal resistance of the condenser. On the other hand, for subsaturated SHLHP with condenser membrane design (as detailed in Figure 3), the effective thermal resistance is reduced to that of the condenser wick and condenser wall material, as discussed in the Design and Operating Principles section (comparison between Figures 2b, c), and the rise in the evaporator temperature is significantly slower than in the saturated systems.

In the predictions for conventional LHP in Figure 5 (with the liquid path taken to be perfectly insulated), the evaporator temperature increases with increasing heat input over the entire power range when no adverse acceleration is imposed ($g_{total} = 0$). When there is adverse acceleration imposed on the system, characteristic u-shaped curves[13,30] appear at the low heat flux. Looking at a single heat input, the higher the adverse acceleration load, the larger the liquid path hydrostatic pressure must be, as required by the temperature head condition (Eq. 3) and shown schematically in Figure 3a. For a fixed acceleration, the increasing heat input leads to increasing flow rate, providing more efficient cooling for the evaporator and reducing the temperature difference in the compensation chamber; as the heat input keeps increasing, the conventional LHP enters its fixed conductance mode where the impact of acceleration becomes small compared to that of the viscous pressure head, and the system is

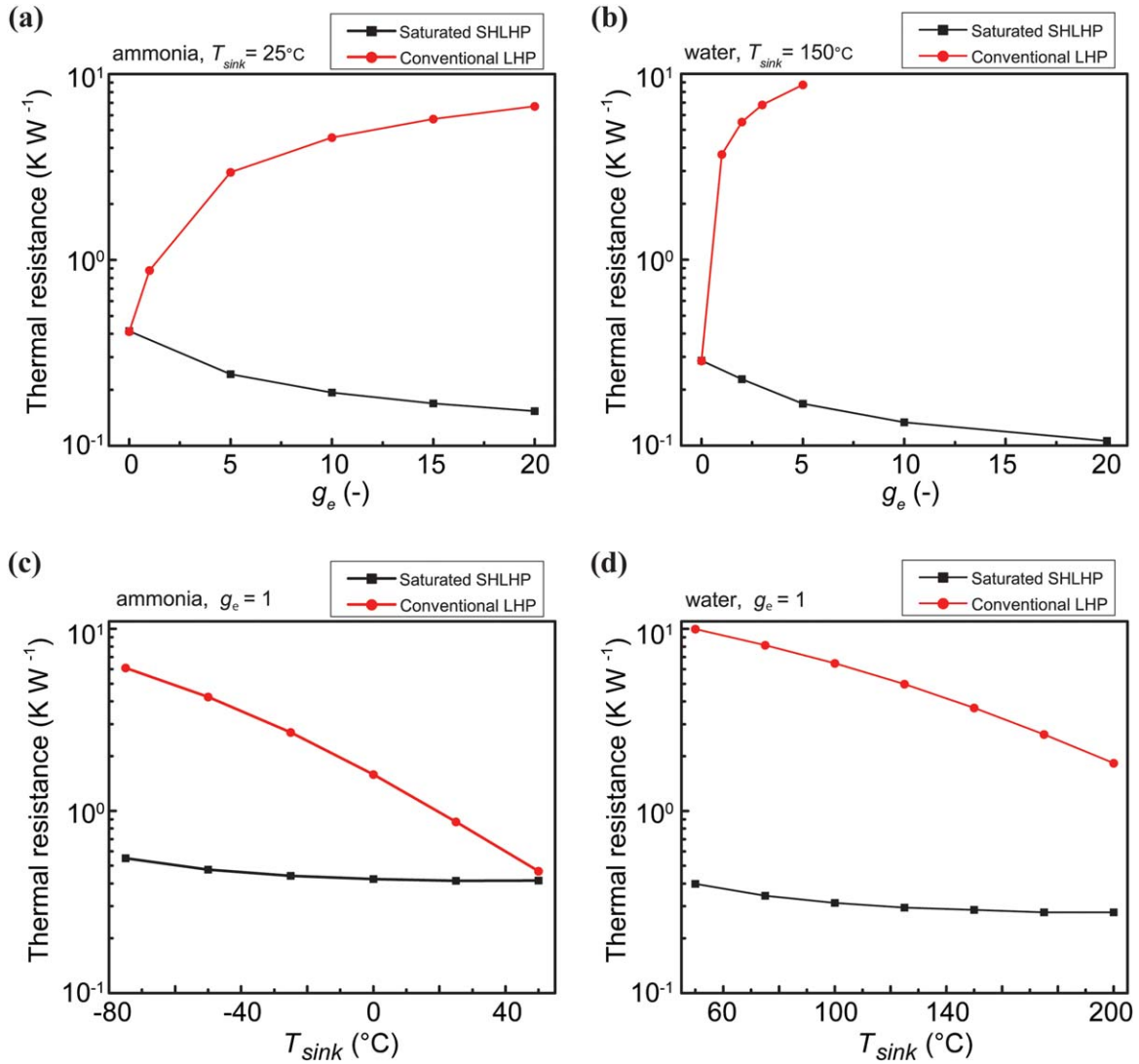

Figure 6. Comparison of the total effective thermal resistance for conventional LHP and saturated SHLHP varying acceleration (a-b) and sink temperature (c-d), with ammonia and water as the working fluid.

Black squares are numerical solutions (Eqs. A1–A9 and Eqs. 7–11) for total effective thermal resistance for subsaturated SHLHPs; red circles are solutions for conventional LHPs. The heat input, $q_i = 10$ W. Sink temperature, T_{sink}, is 25°C for (a) ammonia and 150°C for (b) water. $g_{total} = 1\ g_e$ for both (c) and (d). $L_{pipe} = 10$ m, other operational parameters are the same as in Figure 5. [Color figure can be viewed in the online issue, which is available at wileyonlinelibrary.com.]

dominated by the resistance to heat transfer in the condenser. The larger the acceleration load, the later the operating curve enters the fixed conductance mode.

In summary, while the effective resistance of conventional LHPs is strongly affected by the adverse acceleration due to Eq. 3 and Eq. 4, the resistance of SHLHPs is independent of the pressure load in this range due to the absence of the saturated state in compensation chamber. Further, by eliminating the film resistance in the condenser, the global resistance of a subsaturated SHLHP is predicted to be lower than that in either the saturated SHLHP or the conventional LHP.

Response to acceleration load. Figures 6a, b compare the effective thermal resistances (numerically solved Eqs. A1–A9 and Eqs. 7–11) of a conventional LHP and a saturated SHLHP as a function of the adverse acceleration for ammonia (Figure 6a) and water (Figure 6b) for $q_i = 10$ W. For both fluids, the resistance of the SHLHP is small [R_{film} ~0.4 for (a) and 0.3 for (b)] and varies slowly with g_{total}. The predicted decrease in the resistance with increasing g_{total} comes from the impact of acceleration on the film resistance in the model we have used (Eq. 18). As we will illustrate in the section *Contributions of loop elements to R_{eff} for SHLHPs*, the other resistances are insensitive to acceleration. The resistance of the conventional LHP is much larger than that for the SHLHP for $g_{total} > 0$ and increases with the increasing adverse acceleration; this trend validates the schematic description provided in Figure 3a. At the heat input considered (10 W), the conventional design is operating below its fixed conductance regime (see Figure 5). We note that the impact of increasing acceleration is more pronounced for water than for ammonia at the temperatures considered, due to the weaker slope of water's saturation curve.

Response to sink temperature. Figures 6c, d compare the effective thermal resistances of the two designs as a function of sink temperature for ammonia (Figure 6c) and water (Figure 6d) with $g_{total} = 1\ g_e$ in the adverse orientation. The temperatures for each fluid were chosen to be within their most

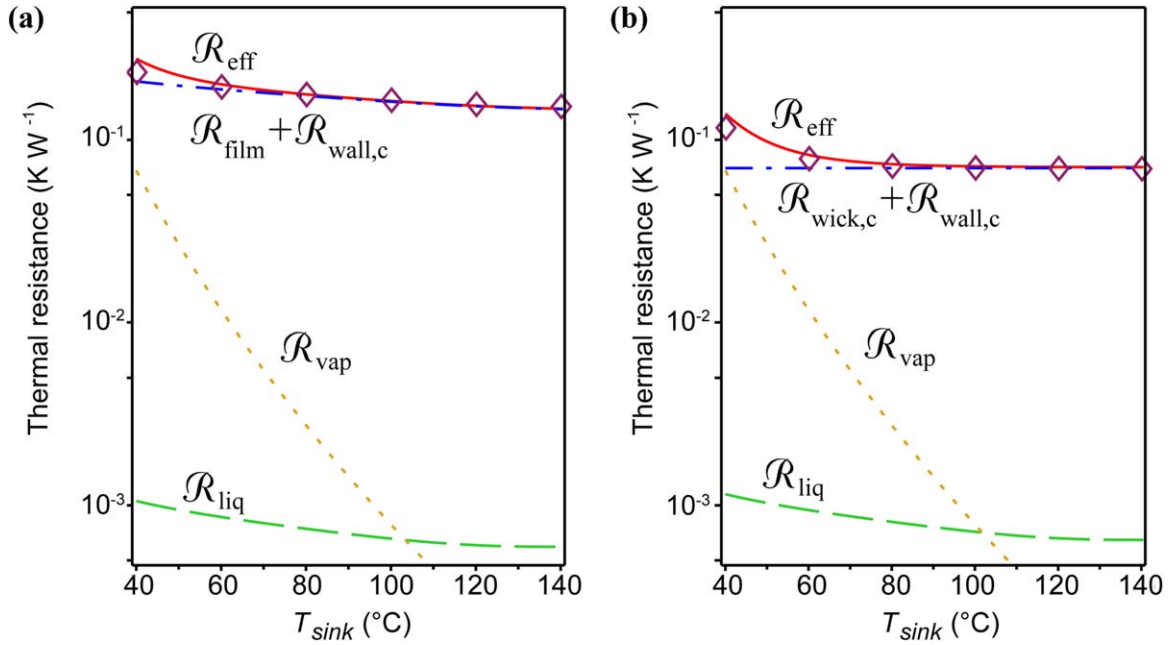

Figure 7. Predicted effective thermal resistances of (a) saturated SHLHP and (b) subsaturated SHLHP as a function of the sink temperature, T_{sink}.

Water is used as the working fluid. Purple diamond symbols are numerical solutions of total effective thermal resistance (Eqs. A1–A9 and Eqs. 7–11) for $q_i = 100$ W. Red solid line is the solution from linearized expression, R_{eff} (Eq. 14), and dashed lines are components of R_{eff} due to different components in the loop—the vapor path is gold, dotted line (R_{vap}, Eq. 19), the liquid path is green, dashed line (R_{liq}, Eq. 20), and the condenser is blue, dash-dot line ($R_{wick,c} + R_{wall,c}$, Eqs. 16 and 15). Operational parameters: $g_{total} = 10\ g_e$ (100 m s^{-2}), $L_{pipe} = 10$ m, $A_{source} = 1$ cm^2, $D_{vap} = 6$ mm, $D_{liq} = 350$ μm, $L_{pore,1} = 2$ μm, $D_{pore,1} = 20$ nm, $L_{pore,2} = 300$ μm, $D_{pore,2} = 2$ μm, and $L_{wall} = 0.5$ mm. For (a), $D_{cond} = 4$ mm, $A_{sink} = 100$ cm^2; for (b), $a_{reg} = 0.99$, $A_w = A_{sink} = 1$ cm^2, $k_w = 130$ W/m K, and $k_{wall} = 400$ W/m K. [Color figure can be viewed in the online issue, which is available at wileyonlinelibrary.com.]

efficient ranges.[13] For both fluids, the resistance of the SHLHP is small [$R_{film} \sim 0.5$ for (c) and 0.4 for (d)] and nearly independent of T_{sink}. The slight rise at the lowest temperatures is due to the resistance to vapor flow, as we will see more clearly in the section *Contributions of loop elements to R_{eff} for SHLHPs*. The resistance of the conventional LHP is much larger than for the SHLHP for all conditions and varies significantly over the ranges of temperature considered. The large effective thermal resistance of the LHP arises from the need to generate sufficient pressure in the vapor at the evaporator to drive the fluid around the loop and against gravity. As discussed in the Design and Operating Principles section (Eq. 3) and shown schematically in Figure 4b, the evaporator temperature must rise until the vapor pressure is sufficiently high to drive the flow; this rise in the T_e^{vap} raises the global thermal resistance for a given, fixed T_{sink}. As T_{sink} increases, the global temperature difference decreases, and the effective resistance falls. The predictions in Figures 6c, d validate the schematic description provided in Figure 3b and illustrate the potential advantages—constant, low thermal resistance over a broad range of sink temperatures—of the SHLHP design.

Validity of SHLHP linear response

To test the predictions of our linear response treatment (Eqs. 14–20) against full numerical solutions of Eqs. A1–A9 and Eqs. 7–11, and to elucidate the relative contributions of distinct components of the system, Figure 7 presents the total thermal resistance of saturated SHLHP (Figure 7a) and subsaturated SHLHP (Figure 7b) with an adverse acceleration of 10 g_e ($g_{total} = 100$ m s^{-2}). Other operational parameters are included in the caption. The symbols in Figure 7 present the full numerical solution for the total effective thermal resistance, R_{eff} (Eqs. A1–A9 and Eqs. 7–11), as a function of T_{sink} for $q_i = 100$ W; the continuous lines are the predictions of the linearization, Eqs. 14–20. For these parameters, the predictions of the linearized equations are in good agreement with the full solutions except at the lowest temperature. We can understand the origin of the breakdown of the linearized theory by noting that among the conditions for the validity of this linearization (Eqs. B2–B7 and B9–B10): Eq. B4 is the first to breakdown for water in the temperature range considered as the rate of heat transfer is increased. When re-expressed in terms of the effective thermal resistance, it requires that

$$q_i \ll \frac{p_{s,0}}{R_{eff}\left.\frac{dp_s}{dT}\right|_{T_0}} \tag{25}$$

for the linearized solution to be valid. This condition fails as the total resistance increases due to the increasing resistance of the vapor path, R_{vap} as the saturation pressure of vapor decreases at low temperatures.

Contributions of loop elements to R_{eff} for SHLHPs

We return to Figure 7 to see the distinct contributions of the components of the SHLHP to the effective thermal resistance. The terms R_{wall}, R_{wick}, and R_{film} are simply the conductive resistance of the wall material, the wick membrane in the condenser, and the heat-transfer resistance for conducting the heat out to the sink. We are particularly interested in the effective thermal resistance due to the resistance to the flow of the vapor and liquid. Despite the substantial hydraulic resistance to liquid flow through a capillary 10-m long and 350 μm in diameter, the contribution of the liquid

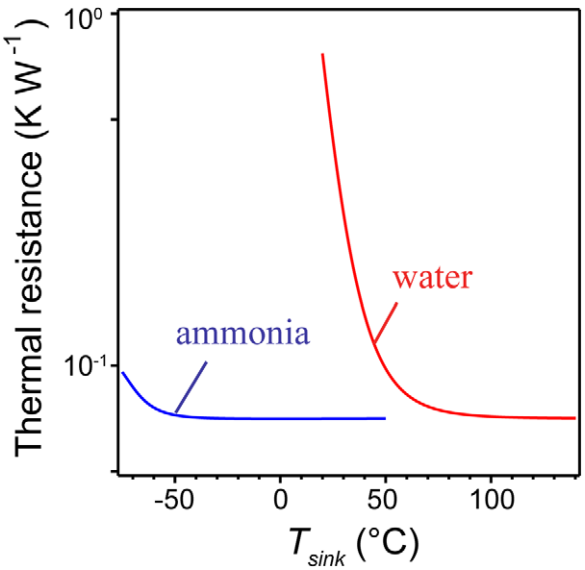

Figure 8. Total effective thermal resistances of subsaturated SHLHP (Eq. 14) with water (red curve) and ammonia (blue curve) as working fluid.

In the range of ambient temperature (−30 to 50°C), ammonia serves as a better working fluid in that its total effective thermal resistance is constant and lower than that of water. $g_{total} = 10$ g_e, $L_{pipe} = 10$ m, other operational parameters are the same as for Figure 7b, provided in the caption of Figure 7. [Color figure can be viewed in the online issue, which is available at wileyonlinelibrary.com.]

path to the total thermal resistance is negligible. This fact allows for the design of long SHLHPs with small volumes of liquid (e.g., ~1 mL of liquid per cm^2 of wick for this 10-m long pipe); the minimization of the volume of liquid is important for weight and for stability of this superheated phase. For SHLHPs, the temperature variation within the working fluid itself is small compared to the temperature drop between the condenser and the sink. The global resistance, R_{eff} is essentially R_{film} (or $R_{wick,c}$) + $R_{wall,c}$, except at low temperatures at which R_{vap} becomes of the same order and affects the total resistance; of course, the magnitude of R_{vap} could be decreased by increasing the size of the vapor conduit. As the operating temperature rises, R_{vap} decreases as the slope of the saturation line increases (Eq. 19) and the total thermal resistance is dominated by the condenser resistance in most of the temperature range. As discussed in the Design and Operating Principles section, the inclusion of regulator and condenser wick membrane adds the $R_{wick,c}$ term but gets rid of R_{film} term by eliminating condensate from the vapor side of the condenser; for the case studied, this change leads to a 10-fold reduction in the global thermal resistance (Figure 7b). The elimination of condensate in the subsaturated SHLHP further allows us to use less condenser area compared to the saturated case. In Figure 7, the condenser area used in the subsaturated case (Figure 7b) was 100 times smaller than in the saturated case (Figure 7a), yet the R_{eff} for subsaturated SHLHP is lower.

The increasing evaporator temperature is accompanied by an increase in the slope of the saturation line, resulting into a decrease of resistance in vapor path, R_{vap}. Therefore, after the operation temperature goes up, the resistance from vapor path eventually becomes small relative to the resistances of both the liquid path and wick membranes. Given that the thermal resistances of these solid components and the liquid path have weak temperature dependence, the effective thermal conductivity becomes nearly constant as temperature increases further, such that the total thermal resistance is dominated by the conductive resistance of the condenser wick and heat sink, $R_{wick,c} + R_{wall,c}$. In summary, as the operational temperature rises, the performance of SHLHP shifts from the monotonically decreasing R_{eff} into higher temperature regime in which the effective thermal conductance becomes temperature independent and controlled only by the conductive resistances of the wick and wall.

The model and expressions for effective resistance provide a unified picture that will allow us to apply our SHLHP designs to extremely broad range of conditions. For example, with appropriate choices of working fluids, we could operate the SHLHP under a wide range of temperatures (around −50 to 100°C) with stable performance (effective thermal resistance <0.1 K W^{-1}). Ammonia is a particularly attractive candidate due to the large slope of its saturation curve around ambient temperature. Figure 8 compares the performances of ammonia-based and water-based subsaturated SHLHP. The predictions indicate that using ammonia as working fluid will lead to higher effective thermal conductivities near ambient; moreover, the system will be operating in the higher temperature regime, providing approximately constant global conductance. The use of water as a working fluid is predicted to be more appropriate for higher temperatures (i.e., $T_{sink} > 70$°C).

Impact of activity pinned by the regulator and negative pressures in the liquid

In the expression of R_{eff} for SHLHPs, there is no dependence on activity controlled by the regulator. Physically, a decrease in the activity of the regulator lowers the vapor pressure in the evaporator and thus lowers the temperature required to evaporate the liquid; a decrease in the activity of the regulator also lowers the pressure of the liquid, such that the temperature required to drive evaporation increases. These two effects tend to cancel each other, such that the total thermal resistances are essentially independent of the activity for slightly subsaturated condition as long as the capillary pressure developed by nanoporous wick is sufficient to sustain large stress in the liquid. For example, in a 10-m long, ammonia-operating subsaturated SHLHP with design parameters the same as those for Figure 7b, variations in T_e^{vap} is less than 10^{-4}°C within the activity range of $0.95 < a_{reg} < 0.99$. As the activity goes below 0.95, the pressure difference between the vapor and liquid at the meniscus of evaporator wick membrane starts to exceed the maximum capillary pressure of 20 nm pores.

Figure 9 shows the variation of liquid pressure as functions of the sink temperature (Figure 9a) and the heat load (Figure 9b) in a subsaturated SHLHP. The reduction of pressure comes from hydraulic resistances, adverse acceleration, and the regulation chamber. In this extreme operation scenario, tens of bars of tension are required to operate the SHLHP; this stress is still small compared to the maximum capillary pressure for pores of 20 nm diameter ($\Delta P_{c,max} > 100$ bars throughout the sink temperature range considered). We note that the tension required is also small compared to the largest tensions achieved with synthetic membrane (~ −70 bars)[19]; further, this degree of tension is of the order of stresses found in many plants. In both cases, continuous transportation of the liquid under tension has been shown.

In Figure 9b, a maximum evaporator heat flux of 500 W/cm^2 can be achieved while the system is still under

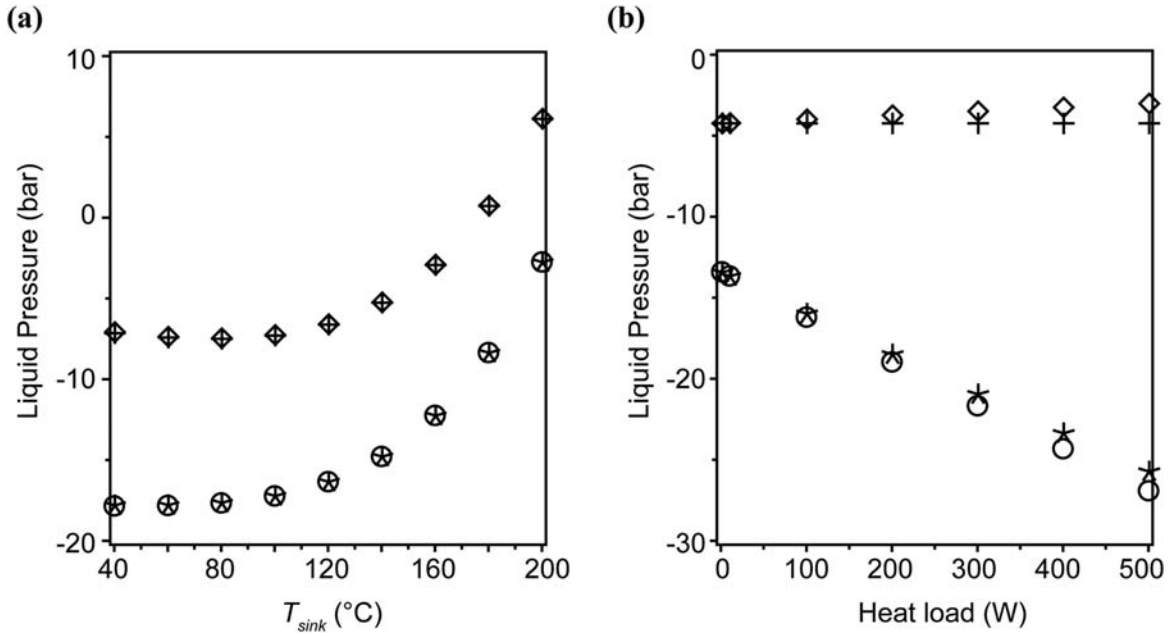

Figure 9. Liquid pressure profile in subsaturated SHLHP as a function of (a) sink temperature, T_{sink}, and (b) heat load.

Diamonds represents the pressure at the condensation surface in the condenser, P_c^{surf}; crosses represent the liquid in the condenser, P_c^{liq}; asterisks represent the pressure in the liquid in the evaporator, P_e^{liq}; and circles represent the pressure at the evaporation surface in the evaporator, P_e^{surf}. The pressure values are calculated from Eqs. A1–A9 and Eqs. 7–10 numerically. $g_{total} = 10\ g_e$, $L_{pipe} = 10$ m, the working fluid is water, $q_i = 10$ W for (a) and $T_{sink} = 150°C$ for (b). Note that 100 W of heat load corresponds to an evaporator heat flux of 100 W/cm^2. Other operational parameters are the same as for Figure 7b, provided in the caption of Figure 7.

subsaturated condition. Under this high heat flux, the Mach number in the vapor path is 0.063, which is far from the sonic limit. Higher heat flux is possible for a SHLHP with lower activity in the regulator; as discussed above, activity controlled by the regulator has negligible effect on the total thermal resistance. Nonetheless, the higher the tension in the liquid, the more the system is prone to cavitation and drying out if defects exist in membranes, as discussed in the following subsection.

Limits of operation of SHLHP

The design of SHLHP could significantly extend the capillary limit as well as eliminate the entrainment and other negative effects of condensate film in the vapor path and the condenser. Nevertheless, the maximum heat flux of SHLHP is subject to constraints including dry-out from the membranes, boiling or cavitation along the liquid path, and choking in the vapor path. The capillary structure in SHLHP is designed to hold large pressure differences between the vapor side and the liquid side of the evaporator. Yet, the maximum capillary pressure will be defined by the largest pore that crosses between the vapor and the liquid sides of the membrane. Any defect, such as a large pore or crack, could compromise the maximum tension achievable before dry-out occurred.

Another underlying challenge is the metastability of liquid under tension.[40,41] As observed in plants, the liquid under negative pressure is vulnerable to cavitation and the subsequent formation of gas-filled (embolized) conduits[42,43]; such events would lead to a dramatic loss of hydraulic transport capacity of the device or even dry-out of the entire liquid path. Both homogeneous nucleation and heterogeneous nucleation of the gas phase can lead to cavitation. One strategy observed in plants to manage and control the spread of cavitation is their segmented xylem structure—a network of conduits separated by rigid plates but hydraulically connected through a large number of bordered pits that traverse the plates.[16] The nanoporous membranes in the center of pits serve as vapor locks that prevent vapor bubbles from expanding beyond the confines of a single conduit. This structure can be mimicked synthetically in a SHLHP, for example, by separating the liquid flow path into individual subunits by nanoporous membranes.

The SHLHP design is prone to the same limitations due to potential choking of the vapor path as in conventional HPs and LHPs.[10] As with conventional LHPs, the choking limit can be avoided by increasing the diameter of the vapor path. For the case of a 10-m long pipe with a 6-mm diameter vapor conduit operating with ammonia at ambient temperature, the Mach number is less than 10^{-1} for heat flows less than 1000 W.

Conclusions

We have analyzed SHLHPs in which nanoporous wick membranes and the absence of a compensation chamber allow for the transport of superheated liquid. We have further proposed the introduction of a regulator to maintain the fluid in a subsaturated state throughout the liquid and vapor paths during operation. Comparing the working cycles of the conventional and the SHLHP designs, we have illustrated that the advantage of SHLHPs are (1) elimination of the temperature head and subcooling conditions that limit the conductance of conventional LHPs and (2) improvement of the condenser thermal conductivity. Our analysis indicates that large hydraulic resistances and large adverse accelerations have negligible impact on the total resistance, such that SHLHPs could be particularly valuable in applications such as cooling of avionics and energy management in buildings in which heat must be transferred over large distances (tens of meters) and against gravity or acceleration (many time gravity). Our analytical expressions for effective resistances provide a valuable

basis for the design of these systems, for example, for the choice of the size of conduits and of the working fluid.

The experimental realization of SHLHPs presents outstanding challenges. The construction of nanoporous membranes must be achieved without introducing excessive hydraulic resistance into the liquid path and in a manner that can support large pressure differences without fracture or collapse. Such structures should couple a thin and uniformly nanoporous layer to hierarchical macroporous supporting layers with increasing diameters and decreasing hydraulic resistances. Another concern about the membrane is that any trace quantities of surfactants or solvents adsorbed to the membrane surface would reduce the effective surface tension (less than the prediction by Eq. 1); suitable choices of membranes and a careful design of fabrication process are needed to minimize the possibility of contamination that may deteriorate the performance of the membranes. The robustness of SHLHP technology depends on the suppression of cavitation in the superheated liquid and the development of means to reconnect the liquid path if cavitation does occur. For the former, pipe wall materials that are hydrophilic and defect free are basic requirements; compartmentalization of the liquid path, as is found in the xylem conduits of plants,[44] could help to control the spread of cavitation. For the later, integration of source of energy to drive refilling must be developed. On all of these fronts, plant physiology may continue to provide significant guidance.[44,45]

Notation

γ = surface tension of the liquid, Pa m
ΔP_c = capillary pressure ($=2\gamma\ cos\theta_c/r_p$), Pa
η_{liq} = viscosity of the condensate, kg m^{-1} s^{-1}]
θ_c = contact angle between the liquid meniscus and the pore wall
λ = heat of vaporization of the working fluid, J kg^{-1}
μ_w^{vap} = chemical potential of the vapor at the vapor-liquid interface, J mole^{-1}
μ_w^{surf} = chemical potential of the liquid at the vapor-liquid interface, J mole^{-1}
$v_{vap,0}$ = kinematic viscosity of the vapor at T_0, m^2 s^{-1}
$v_{liq,0}$ = kinematic viscosity of the liquid at T_0, m^2 s^{-1}
$\rho_{vap,0}$ = density of the vapor at T_0, kg m^{-3}
$\rho_{liq,0}$ = density of the liquid at T_0, kg m^{-3}
A_{source} = area conducting heat into the evaporator, m^2
A_w = area of the wick membrane, m^2
A_{sink} = area conducting heat out of the condenser, m^2
a_{reg} = activity of the regulator
D_{vap} = diameter of the vapor path, m
D_{liq} = diameter of the liquid path, m
D_{cond} = diameter of the condenser tube (for saturated cases), m
D_{pore} = diameter of membrane pores, m
g_{total} = the sum of gravitational and dynamic acceleration, m s^{-2}
g_e = time of gravities ($g_e = 1$, $g_{total} = 10$ kg m s^{-2})
H_e^{vap} = enthalpy of the vapor in the evaporator, J
H_e^{liq} = enthalpy of the liquid in the liquid cavity in the evaporator, J
H_c^{surf} = enthalpy of the liquid at the wick interface in the condenser, J
H_c^{liq} = enthalpy of the liquid in the liquid cavity in the condenser, J
h_{sink} = overall heat-transfer coefficient conducting heat out of the condenser, W m^{-2} K^{-1}
h_{film} = heat-transfer coefficient for the condensate film, W m^{-2} K^{-1}
k_w = effective thermal conductivity of the wick membrane, W m^{-1} K^{-1}
k_{wall} = thermal conductivity of the pipe wall material, W m^{-1} K^{-1}
k_{liq} = thermal conductivity of the condensate, W m^{-1} K^{-1}
L_{pipe} = length of the HP, m
L_{pore} = thickness of the wick membranes, m
L_{wall} = thickness of the pipe wall material, m
MW = molecular weight, kg mole^{-1}
P_e^{surf} = pressure at the surface of the wick membrane of the evaporator, Pa
P_e^{liq} = pressure in the liquid cavity of the evaporator, Pa
P_c^{surf} = pressure at the surface of the wick membrane of the condenser, Pa
P_c^{liq} = pressure in the liquid cavity of the condenser, Pa
$p_s(T)$ = saturation vapor pressure at a given temperature T, Pa
$p_{s,0}$ = saturation vapor pressure at T_0, Pa
p_e = vapor pressures in the vapor cavities of the evaporator, Pa
p_c = vapor pressures in the vapor cavities of the condenser, Pa
Q = mass flow rate of the working fluid, kg s^{-1}
q_i = heat input, W
q_{leak} = heat leaked into the evaporator liquid cavity, W
R_{gas} = the gas constant, J K^{-1} mole^{-1}
Γ_{vap} = hydraulic resistance of the vapor conduit, Pa s kg^{-1}
Γ_{liq} = hydraulic resistances of the liquid conduit, Pa s kg^{-1}
$\Gamma_{wick,e}$ = hydraulic resistance of the wick membrane in the evaporator, Pa s kg^{-1}
$\Gamma_{wick,c}$ = hydraulic resistance of the wick membrane in the condenser, Pa s kg^{-1}
R_{eff} = effective thermal resistance, K W^{-1}
$R_{wall,e}$ = thermal resistance of the evaporator wall, K W^{-1}
$R_{wall,c}$ = thermal resistance of the condenser wall, K W^{-1}
$R_{wick,e}$ = thermal resistance of the evaporator wick membranes, K W^{-1}
$R_{wick,c}$ = thermal resistance of the condenser wick membranes, K W^{-1}
R_{vap} = the contribution associated with the vapor flow within R_{eff}, K W^{-1}
R_{liq} = the contribution associated with the liquid flow within R_{eff}, K W^{-1}
R_{film} = thermal resistance of the film condensation heat transfer, K W^{-1}
r_p = radius of the pores, m
T_{source} = temperatures of the vapor side wall material in the evaporator, K
T_e^{vap} = temperatures in the vapor cavities in the evaporator, K
T_e^{liq} = temperatures in the liquid cavities in the evaporator, K
T_c^{vap} = temperatures in the vapor cavities in the condenser, K
$T_c^{liq}(T_0)$ = temperatures in the liquid cavities in the condenser, K
T_{sink} = temperature of the heat sink outside the liquid side of the condenser, K
$\bar{v}_{liq}$ = molar volume of liquid, m^3 mole^{-1}

Acknowledgments

This work was supported by Air Force Office of Scientific Research (FA9550-09-1-0188) and the graduate fellowship to I.C. from the Corning Foundation.

Literature Cited

1. Wu MS, Liu KH, Wang YY, Wan CC. Heat dissipation design for lithium-ion batteries. *J Power Sources*. 2002;109:160–166.
2. Zalba B, Marín JM, Cabeza LF, Mehling H. Review on thermal energy storage with phase change: materials, heat transfer analysis and applications. *Appl Therm Eng*. 2003;23(3):251–283.
3. Sharma A, Tyagi VV, Chen CR, Buddhi D. Review on thermal energy storage with phase change materials and applications. *Renewable Sustainable Energy Rev*. 2009;13(2):318–345.
4. Pastukhov V, Maidanik YF, Vershinin C, Korukov M. Miniature loop heat pipes for electronics cooling. *Appl Therm Eng*. 2003;23(9): 1125–1135.
5. Garimella SV. Advances in mesoscale thermal management technologies for microelectronics. *Microelectron J*. 2006;37:1165–1185.
6. Pistoia G. *Battery Operated Devices and Systems: From Portable Electronics to Industrial Products*. New York: Elsevier Science Limited, 2009.
7. McCabe WL, Smith JC, Harriott P. *Unit Operations of Chemical Engineering*, *7th ed*. New York: McGraw-Hill Book Company, 2005.
8. Wang G, Mishkinis D, Nikanpour D. Capillary heat loop technology: space applications and recent Canadian activities. *Appl Therm Eng*. 2008;28(4):284–303.
9. Ball P. Computer engineering: feeling the heat. *Nature*. 2012; 492(7428):174–176.
10. Faghri A. *Heat Pipe Science and Technology*. New York: Taylor and Francis, 1995.
11. Ku J. Operating characteristics of loop heat pipes. In: *Proceedings of the International Conference on Environmental System*. Denver, Colorado: Society of Automotive Engineers Inc., SAE transactions 108.1 (1999):503–519.
12. Maydanik YF. Loop heat pipes. *Appl Therm Eng*. 2005;25:635–657.
13. Launay S, Sartre V, Bonjour J. Parametric analysis of loop heat pipe operation: a literature review. *Int J Therm Sci*. 2007;46(7):621–636.

14. Pouzet E, Joly JL, Platel V, Grandpeix JY, Butto C. Dynamic response of a capillary pumped loop subjected to various heat load transients. *Int J Heat Mass Transfer*. 2004;47(10–11):2293–2316.
15. Boure JA, Bergles AE, Tong LS. Review of two-phase flow instability. *Nucl Eng Des*. 1973;25(2):165–192.
16. Nobel PS. *Physicochemical and Environmental Plant Physiology*, *2nd ed*. San Diego, London: Academic Press, 1999.
17. Scholand PF, Hammel HT, Bradstre ED, Hemmingsen EA. Sap pressure in vascular plants—negative hydrostatic pressure can be measured in plants. *Science*. 1965;148(3668):339–346.
18. Choat B, Jansen S, Brodribb TJ, Cochard H, Delzon S, Bhaskar R, Bucci SJ, Feild TS, Gleason SM, Hacke UG. Global convergence in the vulnerability of forests to drought. *Nature*. 2012;491:752–755.
19. Wheeler TD, Stroock AD. The transpiration of water at negative pressures in a synthetic tree. *Nature*. 2008;455(7210):208–212.
20. Kim BH, Peterson GP. Experimental study of a reversible loop heat pipe. *J Thermophys Heat Transfer*. 2005;19(4):519–526.
21. Canham L. *Properties of Porous Silicon, Emisdata Reviews Series*, Vol. 18. London: INSPEC publication, 1997.
22. Bisi O, Ossicini S, Pavesi L. Porous silicon: a quantum sponge structure for silicon based optoelectronics. *Surf Sci Rep*. 2000;38(1–3):1–126.
23. Beale MIJ, Chew NG, Uren MJ, Cullis AG, Benjamin JD. Microstructure and formation mechanism of porous silicon. *Appl Phys Lett*. 1985;46(1):86–88.
24. Guan Y, Fredlund DG. Use of the tensile strength of water for the direct measurement of high soil suction. *Can Geotech J*. 1997;34(4):604–614.
25. Kalsin AM, Fialkowski M, Paszewski M, Smoukov SK, Bishop KJM, Grzybowski BA. Electrostatic self-assembly of binary nanoparticle crystals with a diamond-like lattice. *Science*. 2006;312(5772):420–424.
26. Arora H, Li Z, Sai H, Kamperman M, Warren SC, Wiesner U. Block copolymer directed nanoporous metal thin films. *Macromol Rapid Commun*. 2010;31(22):1960–1964.
27. Winston PW, Bates DH. Saturated solutions for the control of humidity in biological research. *Ecology*. 1960;41(1):232–237.
28. Rockland LB. Saturated salt solutions for static control of relative humidity between 5° and 40°C. *Anal Chem*. 1960;32(10):1375–1376.
29. Kaya T, Hoang TT. Mathematical modeling of loop heat pipes and experimental validation. *J Thermophys Heat Transfer*. 1999;13(3):314–320.
30. Chuang PYA. *An Improved Steady-State Model of Loop Heat Pipes Based on Experimental and Theoretical Analyses. PhD Thesis*. State College, PA: The Pennsylvania State University, 2003.
31. Hamdan M, Cytrynowicz D, Medis P, Shuja A, Gerner FM, Henderson H, Golliher E, Mellott K, Moore C. Loop heat pipe (LHP) development by utilizing coherent porous silicon (CPS) wicks. In: *Proceedings of the Eighth Intersociety Conference on Thermal and Thermomechanical Phenomena in Electronic Systems (ITHERM)*. San Diego, CA: IEEE, 2002, pp. 457–465.
32. Demidov A, Yatsenko ES. Investigation of heat and mass transfer in the evaporation zone of a heat pipe operating by the "inverted meniscus" principle. *Int J Heat Mass Transfer*. 1994;37(14):2155–2163.
33. Cao Y, Faghri A. Conjugate analysis of a flat-plate type evaporator for capillary pumped loops with three-dimensional vapor flow in the groove. *Int J Heat Mass Transfer*. 1994;37(3):401–409.
34. Cotter TP. *Theory of Heat Pipes*, Vol. 37. Los Alamos, NM: Los Alamos National Laboratory, 1965.
35. Launay S, Sartre V, Bonjour J. Analytical model for characterization of loop heat pipes. *J Thermophys Heat Transfer*. 2008;22(4):623.
36. Atkins P, de Paula J. *Physical Chemistry*, *7th ed*. Oxford: Oxford University Press, 2002.
37. Perry RH, Green DW, Maloney JO. *Perry's Chemical Engineer's Handbook*. New York: McGraw-Hill, 1997.
38. Frank PI, David PDW. *Fundamentals of Heat and Mass Transfer*. New York: John Wiley and Sons Inc., 1996.
39. Brennan PJ, Kroliczek EJ. Heat Pipe Design Handbook, Vol. 1. Towson, MD: NASA, 1979.
40. Briggs LJ. Limiting negative pressure of water. *J Appl Phys*. 1950;21(7):721–722.
41. Debenedetti PG. *Metastable Liquids*. Princeton: Princeton University Press, 1996.
42. Tyree MT, Sperry JS. Vulnerability of xylem to cavitation and embolism. *Annu Rev Plant Physiol Plant Mol Biol*. 1989;40(40):19–38.
43. Borghetti M, Grace J, Raschi A. *Water Transport in Plants under Climatic Stress*. Cambridge: Cambridge University Press, 1993.
44. Tyree MT, Zimmermann MH. *Xylem Structure and the Ascent of Sap*, *2nd ed*. Berlin: Springer-Verlag, 2002.
45. Zwieniecki MA, Holbrook NM. Confronting Maxwell's demon: biophysics of xylem embolism repair. *Trends Plant Sci*. 2009;14(10):530–534.

Appendix A: Mass, Heat, and Momentum Balances

Mass balance

At steady state, the system is closed to mass transfer with the outside, thus the mass flow rate, Q, through the liquid and vapor paths is constant. We note that at the startup of the operation, some liquid will be displaced from the liquid path into the vapor path due to thermal expansion as the temperature of the system rises. In the case of saturated SHLHP, we assume that this liquid will collect in the vapor cavity of the condenser; in the case of the subsaturated SHLHP, the excess liquid volume will be evacuated by the regulator such that the vapor path remains devoid of liquid.

Heat balances

The heat input, q_i (W), comes in from the vapor side of the evaporator. We assume perfectly adiabatic liquid and vapor paths such that there is no heat exchange between the pipe lines and the surrounding environment during transportation; all heat that enters at the evaporator exits through at the condenser.

In the evaporator, most of the heat input is used for the liquid vaporization while some of the heat conducts through wick structure in the evaporator into the liquid side; the amount of the heat leakage is proportional to the temperature difference across the wick. Assuming T_{source} is the average temperature of the evaporator wall, $T_{\text{e}}^{\text{vap}}$ is the average temperature in the vapor cavity in the evaporator, and $T_{\text{e}}^{\text{liq}}$ is the average temperature in the liquid cavity in the evaporator, the heat balances in the evaporator vapor side are

$$0 = q_i - \frac{\left(T_{\text{source}} - T_{\text{e}}^{\text{vap}}\right)}{R_{\text{wall,e}}} \tag{A1}$$

and

$$0 = \frac{\left(T_{\text{source}} - T_{\text{e}}^{\text{vap}}\right)}{R_{\text{wall,e}}} - \frac{\left(T_{\text{e}}^{\text{vap}} - T_{\text{e}}^{\text{liq}}\right)}{R_{\text{wick,e}}} - Q\left(H_{\text{e}}^{\text{vap}} - H_{\text{e}}^{\text{liq}}\right) \tag{A2}$$

where $R_{\text{wall,e}}$ (K W^{-1}) represents the thermal resistance between the evaporator wall surface in contact with the heat source and the vapor in the evaporator, and $R_{\text{wick,e}}$ represents the effective thermal resistance of the evaporator wick membrane.

The heat leak into the liquid cavity through the wick casing is neglected (i.e., all the heat leak is conducted through the wick into the liquid side in the evaporator). In the liquid cavity in the evaporator

$$0 = \frac{\left(T_{\text{e}}^{\text{vap}} - T_{\text{e}}^{\text{liq}}\right)}{R_{\text{wick,e}}} - Q\left(H_{\text{e}}^{\text{liq}} - H_{\text{c}}^{\text{liq}}\right) \tag{A3}$$

such that the heat conducted though the wick is balanced by the sensible heat of the cold liquid returning from the condenser (this equation is essentially Eq. 4). The heat exchange between the liquid cavity and ambient is neglected by assuming perfect insulation of the liquid side wall.

For the case of a SHLHP subsaturated throughout the loop, a membrane is used in the condenser and the condensation would occur at the wick surface. An additional heat balance equation is used to describe the heat released by the fluid in the condenser via conduction

though the wick in to the liquid cavity; this heat transfer can be related to the temperature difference across the wick membrane

$$0=Q(H_e^{vap}-H_c^{surf})-\frac{\left(T_c^{vap}-T_c^{liq}\right)}{R_{wick,c}} \quad \text{(subsaturated SHLHPonly)} \tag{A4}$$

where T_c^{vap} is the average temperature in the vapor cavity in the condenser, and T_c^{liq} is the average temperature in the liquid cavity in the condenser. The temperature of the heat sink in contact with the condenser wall is fixed at a constant, known value T_{sink}, such that

$$0=h_{sink}A_{sink}\left(T_c^{liq}-T_{sink}\right)-q_i \tag{A5}$$

where h_{sink} is the overall heat-transfer coefficient and A_{sink} is the heat exchange surface area between the liquid in the condenser and the heat sink. We note that for conventional design, Eq. A5 is a simplified version of the condenser tube energy balance; more detailed model can be found in the literature.[35] This simplification does not affect our results or comparisons between the conventional design and the designs proposed in this article.

Momentum balances

For the liquid phase

$$0=Q\Gamma_{liq}+\rho_{liq}g_{total}L_{pipe}-\left(P_c^{liq}-P_e^{liq}\right) \tag{A6}$$

where g_{total} (m s^{-2}) is the total acceleration along the pipe due to both gravity and acceleration ($g_{total}=g_0+g_{dyn}$, where g_0 and g_{dyn} are the projections of the gravitational and dynamic acceleration onto the axis of the pipe.). For the wick membrane in the evaporator

$$0=Q\Gamma_{wick,e}-\left(P_e^{liq}-P_e^{surf}\right) \tag{A7}$$

For the vapor phase

$$0=Q\Gamma_{vap}+p_c\exp\left(-\frac{MWg_{total}L_{pipe}}{R_{gas}T_e^{vap}}\right)-p_e \tag{A8}$$

The Boltzmann factor in the exponential term accounts for the effect of acceleration, g_{total}, along the axis of the pipe on the vapor.

In the case of conventional LHPs and saturated SHLHPs, pressure losses in the condenser are usually negligible; while for a subsaturated SHLHP, liquid overcomes hydraulic resistance flowing through the condenser wick membrane

$$P_c^{surf}=P_c^{liq} \text{ (conventional LHP and saturated SHLHP)} \tag{A9a}$$

or

$$0=Q\Gamma_{wick,c}-(P_c^{surf}-P_c^{liq}) \text{ (sub-saturated SHLHP)} \tag{A9b}$$

Appendix B: Linear Analysis and Expression of LHP Effective Thermal Resistance

To find the expression of the second term in Eq. 13 for R_{eff}, we use $\Delta T_{tot}=(T_e^{vap}-T_c^{liq})$ and $T_0=T_c^{liq}$. We begin by recasting the local equilibrium at the evaporator, Eq. 7, into a nondimensional form and as an expansion in ΔT_{tot}

$$\frac{p_e\frac{dp_s}{dT}\Big|_{T_0}}{p_{s,0}^2T_0}\left(\Delta T_{tot}\right)^2+\left[\frac{1}{T_0}\left(1-\frac{p_e}{p_{s,0}}\right)-\frac{\frac{dp_s}{dT}\Big|_{T_0}}{\frac{R_{gas}T_0}{\bar{v}_{liq}}}+\frac{p_e\frac{dp_s}{dT}\Big|_{T_0}}{p_{s,0}^2}\right]\Delta T_{tot}+\left[\frac{\left(P_e^{surf}-p_{s,0}\right)}{\frac{R_{gas}T_0}{\bar{v}_{liq}}}+\left(1-\frac{p_e}{p_{s,0}}\right)\right]=0 \tag{B1}$$

In arriving at Eq. B1, we have expanded $p_s\left(T_e^{vap}\right)$ to first order in ΔT_{tot} about T_0, expanded the logarithm to first order in $1-p_e/p_s\left(T_e^{vap}\right)$, and expanded $1/p_s\left(T_e^{vap}\right)$ to first order in $(dp_s/dT|_{T_0})/p_{s,0}$. These approximations hold for the following conditions

$$\Delta T_{tot}\ll 2\frac{\frac{dp_s}{dT}\Big|_{T_0}}{\frac{d^2p_s}{dT^2}\Big|_{T_0}}, \tag{B2}$$

$$\left|1-\frac{p_e}{p_s\left(T_e^{vap}\right)}\right|\ll 1 \tag{B3}$$

and

$$\frac{\Delta T_{tot}}{p_{s,0}/\frac{dp_s}{dT}\Big|_{T_0}}\ll 1 \tag{B4}$$

If we further assume

$$\frac{\Delta T_{tot}}{T_0}\ll 1 \tag{B5}$$

$$\left|1-\frac{p_e}{p_{s,0}}\right|\ll 1 \tag{B6}$$

and

$$\frac{\frac{dp_s}{dT}\Big|_{T_0}}{\frac{R_{gas}}{\bar{v}_{liq}}}\ll 1 \tag{B7}$$

we can simplify Eq. B1 by neglecting terms that are the product of two small factors and solve for ΔT_{tot}

$$\Delta T_{tot}=-\frac{p_{s,0}^2}{\frac{dp_s}{dT}\Big|_{T_0}}\left[\frac{\left(P_e^{surf}-p_{s,0}\right)}{\frac{R_{gas}T_0}{\bar{v}_{liq}}p_e}+\left(\frac{1}{p_e}-\frac{1}{p_{s,0}}\right)\right] \tag{B8}$$

By differentiating ΔT_{tot} with respect to q_i (i.e., looking for the dependence of p_e and P_e^{surf} on q_i) and assuming the following

$$\frac{\left(P_e^{surf}-p_{s,0}\right)}{\frac{R_{gas}T_0}{\bar{v}_{liq}}}\ll 1 \tag{B9}$$

and

$$\frac{MWg_{total}L_{pipe}}{R_{gas}T_e^{vap}}\ll 1 \tag{B10}$$

we arrive at the expression of R_{eff} in which we can separate out the contributions associated with the vapor flow, R_{vap} (Eq. 19), the liquid flow, R_{liq} (Eq. 20), the conduction through the wicks in the condenser, $R_{wick,c}$ (Eq. 16).

Manuscript received May 22, 2013, and revision received Oct. 19, 2013.